Influence of cold forging and annealing on microstructure and mechanical properties of a high-Mn TWIP steel

P. Kusakin[1]*, A. Kalinenko[1], K. Tsuzaki[2], A. Belyakov[1], R. Kaibyshev[1]

[1]*Belgorod State University, Pobeda 85, Belgorod 308015, Russian Federation*
[2]*Kyushu University, Department of Mechanical Engineering, Fukuoka 819-0395, Japan*

Abstract

The influence of cold biaxial forging and annealing on the microstructure evolution and mechanical properties of Fe-18Mn-0.6C-0.1N TWIP steel was investigated. The microstructure after thermomechanical treatment was examined by means of scanning electron microscopy (SEM) with electron back-scatter diffraction (EBSD) analyzer and transmission electron microscopy (TEM). The microstructure containing a high density of deformation twins was evolved by cold forging. Then, the deformation microstructure was recovered or partially recrystallized during subsequent annealing for 1 h at 673 or 873 K, respectively. The cold biaxial forging followed by partial recrystallization resulted in a very attractive combination of mechanical properties. The yield strength and the ultimate tensile strength of the steel after cold biaxial forging were 1320 and 1540 MPa, respectively, with elongation of 6 %. On the other hand, the yield and ultimate tensile strengths of 770 and 1110 MPa, respectively, and elongation about 40 % were obtained after partial recrystallization. The as-forged and recovery annealed samples showed fatigue limit of 600 and 550 MPa, respectively, and the sample after partial recrystallization showed slightly lower fatigue limit of 500 MPa.

K e y   w o r d s: TWIP-steel, deformation twinning, microstructure, mechanical properties, fatigue

1. Introduction

High-Mn steel with twinning induced plasticity effect (TWIP) has captured the industry attention due to its excellent combination of mechanical properties [1–3]. The TWIP-effect is attributed to the formation of deformation twins with nanometer thickness. The deformation twinning develops in steel with medium stacking fault energy ranging from 20 to 40 mJ m^{-2} [4], which in turn depends on the chemical composition. The extensive formation of nanotwins leads to the so-called dynamic Hall-Petch effect resulting in an exceptionally high strain hardening [5]. Despite great advantages of TWIP steels, they have one common shortcoming that is low yield strength in comparison with modern high strength steels. The yield strength can be improved in several different ways, e.g. cold working followed by heat treatment. Some work on recovery annealing of cold worked steels

[6, 7] proved this method to be useful to enhance strength-plasticity combination. The closely spaced twin boundaries, which were produced by deformation twinning during cold rolling, remain almost unchanged during recovery annealing and, hence, contribute to the yield strength, while lowered dislocation density due to recovery promotes the plasticity. Fatigue limit is one of the most important criteria determining the quality of components and structures. More than 90 % of all fractures are caused by fatigue in service. Numeral works have been carried out to study the recrystallization kinetics and texture after thermomechanical treatment and their effect on the tensile strength [8, 9], but only a little attention has been paid to fatigue resistance of cold worked and annealed high-Mn steel with TWIP-effect [10–13].

The present work aims to obtain more data on structure-property relation including fatigue behavior of TWIP steels subjected to cold working followed by

---

T a b l e 1. Chemical composition of the investigated steel
in wt.%

C	Mn	Al	Si	N	S	P	Fe
0.58	17.9	0.044	0.033	0.083	0.004	0.007	bal.

recovery and partial recrystallization. Biaxial forging
was selected as an advanced technique for processing
of austenitic steels [14–16].

2. Experimental

A high-Mn TWIP steel with a nominal chem-
ical composition given in Table 1 denoted as Fe-
-18Mn-0.6C-0.1N was solution annealed at 1273 K
for 4 h and then forged at 1273 K followed by air
cooling. Then, the steel samples with dimensions of
$15 \times 25 \times 100\,\mathrm{mm}^3$ were subjected to biaxial forg-
ing (BF) at room temperature with a pass strain of
about 0.25; the total true strain was about 0.5. Some
forged samples were annealed at 673 K (BF + A400C)
or 873 K (BF + A600C) for 1 h. For structural char-
acterization, the thin foils of 3 mm diameter were cut
out parallel to the final compression axis and ground
to 0.1 mm thickness. Then, the discs were polished us-
ing a double-jet TENUPOL-5 electrolytic polisher at
a voltage of 20 V at room temperature using an elec-
trolyte containing 10 % perchloric acid and 90 % acetic
acid. The foils were examined using a JEOL JEM-2100
transmission electron microscope (TEM) operated at
an acceleration voltage of 200 kV. The crystallographic
features of the microstructure were determined us-
ing high-resolution electron back-scatter diffraction
(EBSD) with a Quanta 600FEG scanning electron mi-
croscope. The orientation imaging microscopy (OIM)
micrographs were obtained on the different areas of
the longitudinal sections with a scan step of 50 nm
and then subjected to a cleanup procedure, setting
the minimal confidence index to 0.1. The specimens
for tensile tests and fatigue tests were cut out from
cold forged and annealed samples. The tensile tests
were carried out on the flat specimens with the gage
length of 12 mm, a width of 3 mm and a thickness of
1.5 mm. The tensile tests were performed at a constant
rate of $2\,\mathrm{mm\,min^{-1}}$. At least 2 samples were tested to
obtain each data point. For fatigue tests, cylindrical
specimens with a diameter of 5 mm and a gage length
of 25 mm were used. Fatigue tests were carried out
with an asymmetric loading cycle with a minimum to
the maximum tension ratio $R = 0.1$. The tests were
conducted using a universal servo-hydraulic testing
machine Instron 8801. The cyclic load frequency was
50 Hz.

3. Microstructure evolution

Cold biaxial forging with 0.5 true strain resulted
in the development of twinned microstructure as can
be seen in Figs. 1a and 2a. The deformation twins
formed as ~ 2 micron thick bundles (Fig. 1a) with in-
dividual twin thickness of 20 nm (Fig. 2a). The heat
treatment at 673 K for 1 h did not change remarkably
the structure evolved during biaxial forging, indicat-
ing that the recovery processes only took place. Fig-
ure 1b shows the austenite grains with deformation
twins similar to those in Fig. 1a. Figure 2b represents
a TEM image of the twinned area of the specimen
annealed at 673 K. It is clearly seen in Fig. 2b that
the deformation twins belonging to different twinning
systems remain unchanged during recovery anneal-
ing at 673 K. An increase in the annealing tempera-
ture to 873 K resulted in the partially recrystallized
structure as shown in Fig. 1c. The new fine austenitic
grains with quite a low dislocation density, as well as
work hardened regions with high density of deforma-
tion twins were found in the microstructure after 1 h
annealing at 873 K (Fig. 2c). The total fraction of re-
crystallized grains in the specimen annealed at 873 K
was found to be about 10 %, and the mean size of
recrystallized grains was $2 \pm 0.5\,\mu\mathrm{m}$.

Figures 1d–f represent the kernel average misorien-
tation (KAM) maps for OIM micrographs in Figs. 1a–
c. The color-scale-coded KAM maps are plotted on the
basis of the first neighbor kernel parameter with a
maximum misorientation angle of 5°. The blue color
displays misorientations less than 1°, green between
1° and 2°, yellow between 2° and 3°, orange between
3° and 4°, and red between 4° and 5°. The KAM map
of the sample subjected to biaxial forging (Fig. 1d)
reveals the large internal distortions. The huge areas
of yellow to red colors in Fig. 1d indicate the high
dislocation densities corresponding to work hardening
by cold biaxial forging. Annealing at 673 K during 1 h
led to recovery processes, which is proved in Fig. 1e by
large "blue-green" areas with kernel average misorien-
tation less than 2°. After 873 K annealing during 1 h,
the "blue" areas in KAM map expanded while "red"
areas almost disappeared (Fig. 1f) that indicates re-
markable release of internal distortions and disloca-
tions. Moreover, the new grains, which are almost free
of any internal distortions (left-bottom in Fig. 1f), de-
veloped in this sample as a result of partial recrystal-
lization.

4. Mechanical properties

The present Fe-18Mn-0.6C-0.1N TWIP steel in the
initial state showed the yield strength (YS) and the ul-
timate tensile strength (UTS) of 325 and 780 MPa, re-
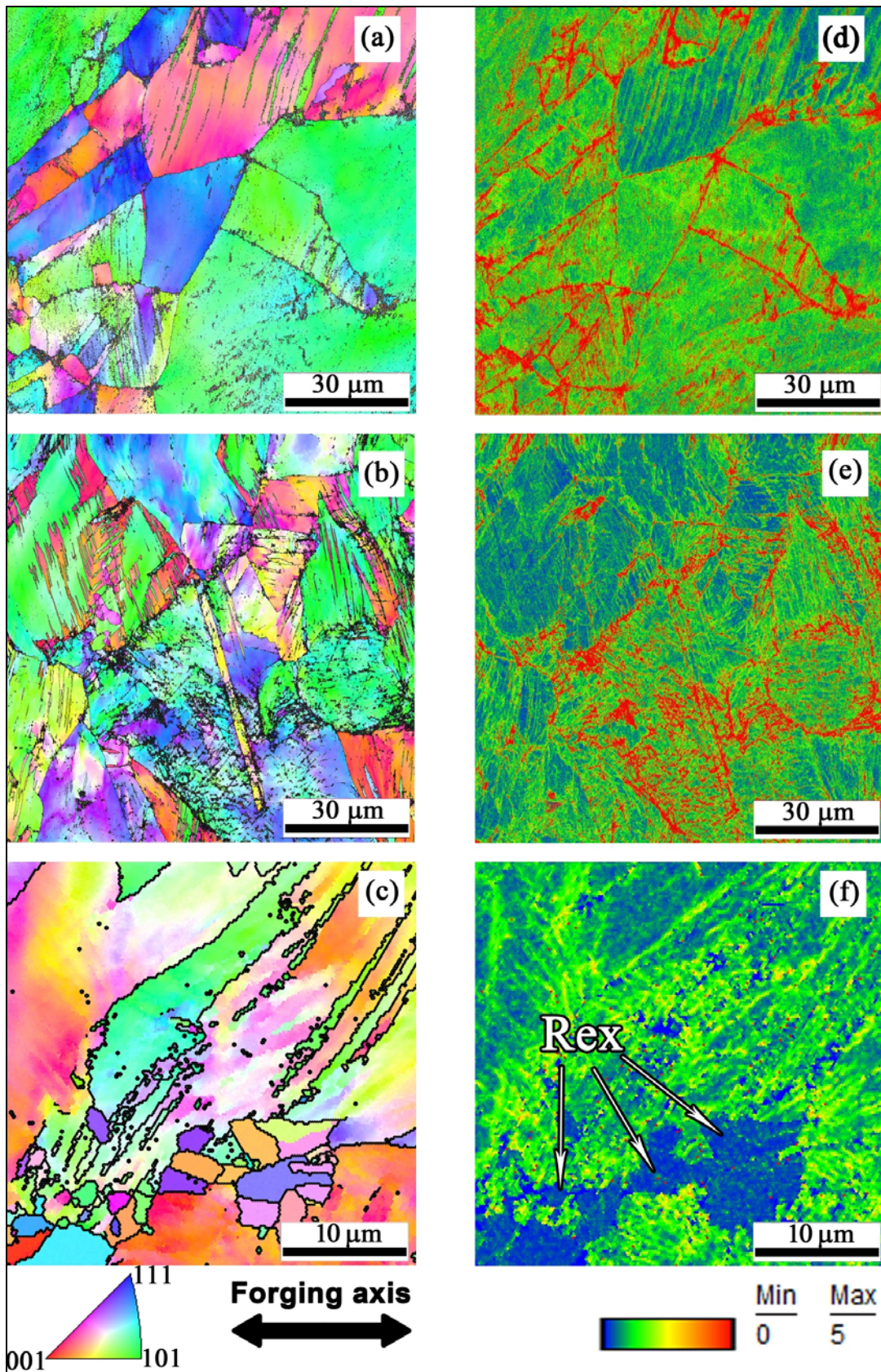spectively, and total elongation of 47 %, which was al-

Fig. 1. OIM micrographs (a–c) and KAM maps (d–f) of microstructures and the distribution of the grain boundary misorientations developed in Fe-18Mn-0.6C-0.1N steel through: (a) biaxial forging (BF), (b) biaxial forging and annealing at 673 K (BF + A400C); (c) biaxial forging and annealing at 873 K (BF + A600C). The inverse pole figures are indicated by the forging axis. The arrows in (f) indicate recrystallized grains.
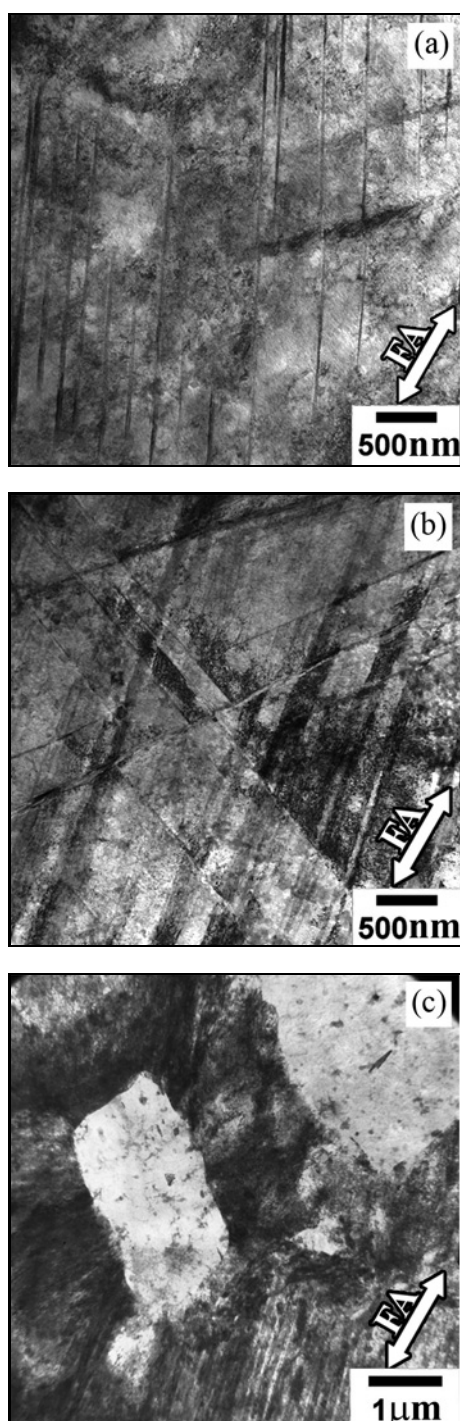
Fig. 2. TEM images of microstructures developed by (a) BF, (b) BF + A400C, (c) BF + A600C. FA indicates the axis of the last forging pass.
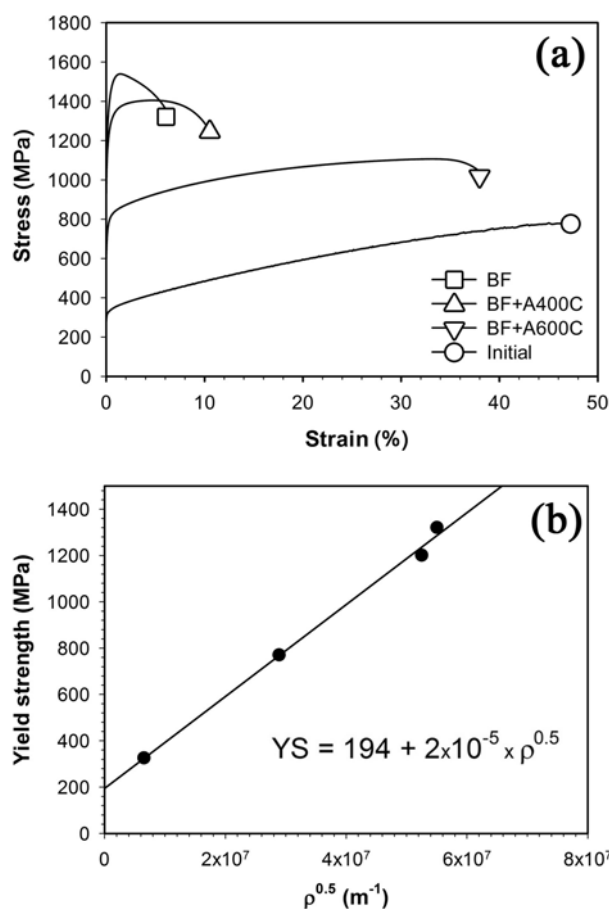

Fig. 3. (a) Stress-strain curves and (b) yield strength vs. square root of dislocation density plots for Fe-18Mn-0.6C-0.1N steel specimens after different thermomechanical treatments.

most uniform as can be seen in Fig. 3a. The cold forged sample showed quite a small uniform elongation and necked just after reaching the yield point. The yield strength and the ultimate tensile strength of the steel after cold biaxial forging were 1320 and 1540 MPa, respectively, while the total elongation was 6 %. Recov-

ery annealing at 673 K of the forged material resulted in a small decrease in the yield strength and the ultimate tensile strength to 1200 and 1410 MPa, respectively, and the total elongation increased to 10 %. An increase of annealing temperature to 873 K resulted in a quite interesting combination of mechanical properties. Namely, the yield strength was 770 MPa; the ultimate tensile strength was 1110 MPa and the elongation comprised about 40 % with uniform elongation of about 35 % (Fig. 3a).

The strengthening of metallic materials during cold working is generally attributed to an increase in the dislocation density [17]. The dislocation densities in the present steel samples can be estimated from kernel average misorientation data obtained from EBSD images using Frank's equation, Eq. (1):

$$\theta \approx 2\sin\frac{\theta}{2} = \frac{Nb}{h}, \qquad (1)$$

where θ is the misorientation created by a wall consisting of N dislocations of height h, and b is the Burgers

Table 2. Values of physical parameters in Eq. (3) and calculated dislocation density

Specimen	θ/h (m^{-1})	b (m)	ρ (m^{-2})
Initial	5.45×10^5	2.54×10^{-10}	4.3×10^{13}
BF	3.84×10^7	2.54×10^{-10}	3×10^{15}
BF + A400C	3.5×10^7	2.54×10^{-10}	2.75×10^{15}
BF + A600C	1.06×10^7	2.54×10^{-10}	8.4×10^{14}

Table 3. Values of physical parameters in Eq. (6)

α	M	G (MPa)	b (m)	σ_0 (MPa)
0.36	3	72000	2.54×10^{-10}	194

vector. In EBSD experiments, distance h corresponds to the step size of the scanning. The dislocation density ρ is then given by the ratio of the dislocation number per surface area, Eq. (2):

$$\rho = \frac{N}{S},\qquad(2)$$

where the surface area of the hexagon S (scanning geometry) is $S = \sqrt{3}h^2/2$. It follows that the dislocation density can be estimated from the following relationship:

$$\rho = \frac{2\theta}{\sqrt{3}hb}.\qquad(3)$$

The values used for dislocation density calculations are given in Table 2.

The relationship between the yield strength and the dislocation density of the Fe-18Mn-0.6C-0.1N steel is displayed in Fig. 3b. The yield strength (YS) shows a linear dependence on the dislocation density square root and can be expressed as follows:

$$\text{YS} = 194 + 2 \times 10^{-5}\sqrt{\rho}.\qquad(4)$$

Generally, the flow stress in terms of the resolved shear stress (τ) relates to the square root of dislocation density [17, 18]:

$$\tau = \tau_0 + \alpha Gb\sqrt{\rho},\qquad(5)$$

where τ_0 is the friction stress, α is a constant, G is the shear modulus, and b is Burgers vector. In terms of tensile stress, taking $\sigma = M\tau$, the flow stress (σ) is estimated by the following relationship:

$$\sigma = \sigma_0 + \alpha MGb\sqrt{\rho},\qquad(6)$$

where M is the average Taylor factor. Then, the coefficients in Eq. (4) can be expressed in terms of parameters used in Eq. (6). The values of these physical parameters used in Eq. (6) for Fe-18Mn-0.6C-0.1N
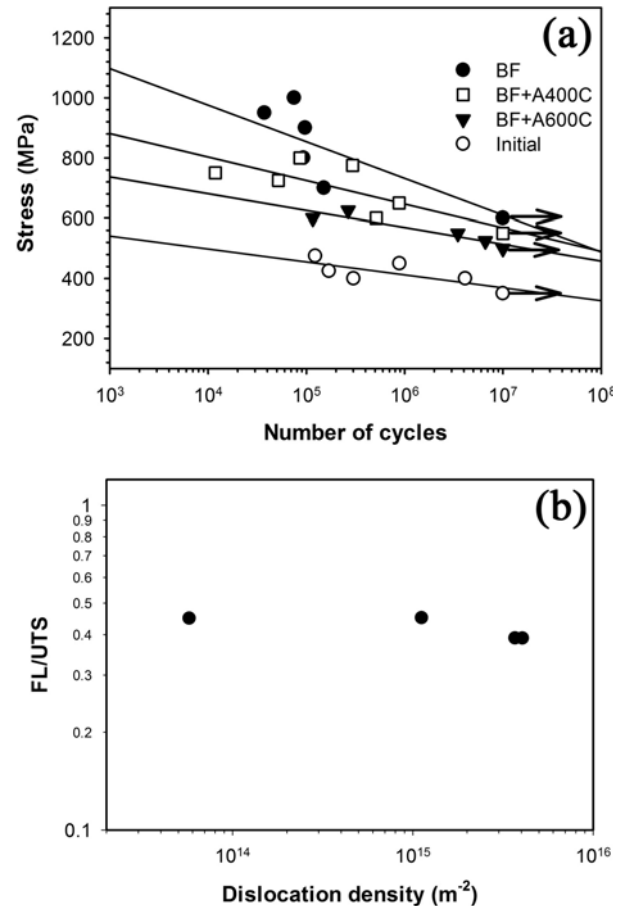

Fig. 4. (a) Stress amplitude-fatigue life data and (b) fatigue limit normalized by ultimate tensile strength (FL/UTS) as a function of dislocation density of Fe-18Mn-0.6C-0.1N steel specimens after different thermomechanical treatments. The arrows in (a) indicate no failure at given stress amplitude after 10^7 cycles.

TWIP steel are given in Table 3. The numerical factor of $\alpha = 0.36$ is almost the same as those reported in other theoretical and experimental studies on dis-

location strengthening [19–21]. This suggests that the yield strength of the present steels with different microstructures, i.e. work hardened, recovery annealed and partially recrystallized, can be expressed by a unique function of dislocation strengthening.

Figure 4a shows the experimental fatigue data for the Fe-18Mn-0.6C-0.1N steel. The specimens in the initial state showed fatigue limit (FL) of 350 MPa corresponding to 10^7 cycles. The specimens with as-forged and recovered structures exhibited fatigue limits of 600 and 550 MPa, respectively, while the specimen after partial recrystallization is characterized by a slightly lower fatigue limit of 500 MPa.

It can be seen from the fatigue data in Fig. 4a that the recovered structure provides lower fatigue resistance at cycle number below 10^7 cycles. As the deformation twins remain stable until recrystallization [22–24], the difference between these two conditions is the dislocation density only. Therefore, the dislocation density affects remarkably the fatigue resistance in work hardened and recovered TWIP steels.

Figure 4b represents the relationship between the fatigue limit normalized by ultimate tensile strength (FL/UTS) and the dislocation density. Commonly, the fatigue limit of steels can be roughly related to the tensile strength, so that the ratio of FL/UTS is generally between 0.4 and 0.6 [25]. This rule is applicable to all the present steel samples subjected to cold forging and various annealing treatments as can be seen in Fig. 4b. It is worth noting that despite large differences in processing conditions and the dislocation densities, the FL/UTS ratio remains almost unchanged and stays in the range of 0.42 ± 0.03 that is slightly lower than values reported for different TWIP-steels in recrystallized conditions [12].

5. Summary

The influence of cold forging and annealing on the microstructure evolution and mechanical properties of a high-Mn TWIP steel (Fe-18Mn-0.6C-0.1N) was investigated. The main conclusions can be drawn as follows:

1. Cold biaxial forging with a total true strain of 0.5 resulted in the development of twinned microstructure with a high dislocation density of $3 \times 10^{15}\,\mathrm{m}^{-2}$. The deformation twins formed as ~ 2 micron thick bundles with individual twin thickness of 20 nm. The heat treatment at 673 K for 1 h favored only recovery processes, whereas annealing at 873 K resulted in partially recrystallized microstructure with a grain size of 2 microns and their fraction of 0.1.

2. The steel showed YS = 325 MPa and UTS = 780 MPa with total elongation of 47 % in the initial state and YS = 1320 MPa, UTS = 1540 MPa with the total elongation of 6 % after multiple-stage cold forg-

ing. Recovery annealing of the forged material resulted in a decrease of YS and UTS to 1200 and 1410 MPa, respectively, and the total elongation increased to 10 %. Further increase of annealing temperature resulted in an attractive combination of mechanical properties: YS = 770 MPa, UTS = 1110 MPa with uniform elongation about 35 %. The yield strength of the steel in different conditions can be described as follows: $\mathrm{YS} = 194 + 2 \times 10^{-5}\sqrt{\rho}$.

3. The steel in the initial state showed FL = 350 MPa at 10^7 cycles. As-forged and recovered specimens showed FL of 600 MPa and 550 MPa at 10^7 cycles, respectively. The specimen after partial recrystallization showed slightly lower FL of 500 MPa. The FL/UTS ratio of 0.42 ± 0.03 remains almost unchanged.

References

[1] Bouaziz, O., Allain, S., Scott, C. P., Cugy, P., Barbier, D.: Curr. Opin. Solid State Mater. Sci., *15*, 2011, p. 141. doi:10.1016/j.cossms.2011.04.002

[2] Chen, L., Zhao, Y., Qin, X.: Acta Metall. Sin. (English Lett.), *26*, 2013, p. 1. doi:10.1007/s40195-012-0501-x

[3] Kim, H.-S., Suh, D.-W., Kim, N. J.: Sci. Technol. Adv. Mater., *14*, 2013, 014205. doi:10.1088/1468-6996/14/1/014205

[4] Dumay, A., Chateau, J.-P., Allain, S., Migot, S., Bouaziz, O.: Mater. Sci. Eng. A, *483–484*, 2008, p. 184. doi:10.1016/j.msea.2006.12.170

[5] Bouaziz, O., Guelton, N.: Mater. Sci. Eng. A, *319–321*, 2001, p. 246. doi:10.1016/S0921-5093(00)02019-0

[6] Haase, C., Barrales-Mora, L. A., Molodov, D. A., Gottstein, G.: Metall. Mater. Trans. A, *44*, 2013, p. 4445. doi:10.1007/s11661-013-1935-0

[7] Bouaziz, O., Scott, C. P., Petitgand, G.: Scr. Mater., *60*, 2009, p. 714. doi:10.1016/j.scriptamat.2009.01.004

[8] Haase, C., Barrales-Mora, L. A., Roters, F., Molodov, D. A., Gottstein, G.: Acta Mater., *80*, 2014, p. 327. doi:10.1016/j.actamat.2014.07.068

[9] Koyama, M., Lee, T.-Y., Lee, C. S., Tsuzaki, K.: Mater. Des., *49*, 2013, p. 234. doi:10.1016/j.matdes.2013.01.061

[10] Nikulin, I., Sawaguchi, T., Tsuzaki, K.: Mater. Sci. Eng. A, *587*, 2013, p. 192. doi:10.1016/j.msea.2013.08.061

[11] Hamada, A. S., Karjalainen, L. P., Puustinen, J.: Mater. Sci. Eng. A, *517*, 2009, p. 68. doi:10.1016/j.msea.2009.03.039

[12] Hamada, A. S., Karjalainen, L. P., Ferraiuolo, A., Gil Sevillano, J., de las Cuevas, F., Pratolongo, G., Reis, M.: Metall. Mater. Trans. A, *41*, 2010, p. 1102. doi:10.1007/s11661-010-0193-7

[13] Hamada, A. S., Karjalainen, L. P.: Mater. Sci. Eng. A, *527*, 2010, p. 5715. doi:10.1016/j.msea.2010.05.035

[14] Tikhonova, M., Belyakov, A., Kaibyshev, R.: Mater. Sci. Eng. A, *564*, 2013, p. 413. doi:10.1016/j.msea.2012.11.088

[15] Yanushkevich, Z., Mogucheva, A., Tikhonova, M., Belyakov, A., Kaibyshev, R.: Mater. Charact., *62*, 2011, p. 432. doi:10.1016/j.matchar.2011.02.005

[16] Shakhova, I., Dudko, V., Belyakov, A., Tsuzaki, K., Kaibyshev, R.: Mater. Sci. Eng. A, *545*, 2012, p. 176. doi:10.1016/j.msea.2012.02.101

[17] Gottstein, G.: Physical Foundations of Materials Science. Berlin, Heidelberg, Springer 2004. doi:10.1007/978-3-662-09291-0

[18] Kocks, U. F., Mecking, H.: Prog. Mater. Sci., *48*, 2003, p. 171. doi:10.1016/S0079-6425(02)00003-8

[19] Allain, S., Chateau, J.-P., Bouaziz, O.: Mater. Sci. Eng. A, *387*, 2004, p. 143. doi:10.1016/j.msea.2004.01.060

[20] Soulami, A., Choi, K. S., Shen, Y. F., Liu, W. N., Sun, X., Khaleel, M. A.: Mater. Sci. Eng. A, *528*, 2011, p. 1402. doi:10.1016/j.msea.2010.10.031

[21] Chinh, N. Q., Horváth, G., Horita, Z., Langdon, T. G.: Acta Mater., 2004, *52*, p. 3555. doi:10.1016/j.actamat.2004.04.009

[22] Kang, S., Jung, Y.-S., Jun, J.-H., Lee, Y.-K.: Mater. Sci. Eng. A, *527*, 2010, p. 745. doi:10.1016/j.msea.2009.08.048

[23] Dini, G., Najafizadeh, A., Ueji, R., Monir-Vaghefi, S. M.: Mater. Lett., *64*, 2010, p. 15. doi:10.1016/j.matlet.2009.09.057

[24] Viscorova, R., Kroos, J., Flaxa, V., Wendelstorf, J., Spitzer, K. H.: In: Proceedings of IDDRG Conference. Ed.: Kergen, R. Düsseldorf, Verlag Stahleisen GmbH 2004, p. 261. ISBN 3-514-00708-X.

[25] Chapetti, M. D., Miyata, H., Tagawa, T., Miyata, T., Fujioka, M.: Mater. Sci. Eng. A, *381*, 2004, p. 331. doi:10.1016/j.msea.2004.04.055